Optimization of Bit Geometry and Multi-Reader Geometry for TDMR

John R. Barry[1], Bane Vasić[2], Mehrdad Khatami[2], Mohsen Bahrami[2],
Yasuaki Nakamura[3], Yoshihiro Okamoto[3], and Yasushi Kanai[4]
[1]School of Electrical and Computer Engineering, Georgia Institute of Technology, Atlanta, GA 30332-0250 USA
[2]Department of Electrical and Computer Engineering, University of Arizona, Tuscon, AZ 85721 USA
[3]Graduate School of Science and Engineering, Ehime University, Matsuyama 790-8577 Japan
[4]Department of Information and Electronics Engineering, Niigata Institute of Technology, Kashiwazaki 945-1195, Japan

The move from traditional single-track magnetic recording to TDMR with squeezed tracks and multiple readers opens up new design degrees of freedom beyond the track pitch and bit aspect ratio, including the widths, spacing, and crosstrack positions of the readers. In this paper we present a systematic method for determining the combination of multiple-reader geometry, track pitch, and bit-aspect ratio that maximizes the areal density of a TDMR system using single-track detectors. The method combines realistic modeling of the medium and write/read processes, advanced signal detection, and information-theoretic tools. The two-reader geometry that maximizes areal density with zero skew and zero misregistration was found to use different-sized readers (with widths of 14.6 nm and 23.9 nm) with significant overlap in the crosstrack direction (centers spaced by 2 nm). The optimal track pitch was 16.1 nm and the optimal bit length was 7.3 nm. At the optimal operating point, the information rate per coded bit is 0.8.

***Index Terms*—Two-dimensional magnetic recording, shingled magnetic recording, intersymbol interference (ISI), intertrack interference (ITI), data-dependent noise, information theory**

I. Introduction

TWO-dimensional magnetic recording (TDMR) is an accepted part of the industry's technology roadmap for hard disk drives [1]–[3]. The first implementations of TDMR will likely use just two closely spaced stacked readers on tracks written using shingled magnetic recording [4]. The optimization of a conventional single-track recording system is a complex process involving many parameters. The optimization of a dual-reader TDMR system is still more complex involving at least three additional parameters: the two reader widths and the cross-track offset (or spacing) between the readers.

This paper examines the optimization of a dual-reader TDMR system to maximize customer areal-density at a fixed radius and velocity. (The change in cross-track offset as a function of radius/skew for a stacked reader is not dealt with here.) The search for the optimum is conducted over the following six parameters: track pitch, channel/media linear density, reader-1 width, reader-2 width, reader-1 position, and reader-2 position.

The optimization is done through software processing of waveforms derived from a quasi-static recording simulation of long pseudo-random bit sequences [5]. An important part of this work is the verification that the simulated waveforms are realistic and representative. The signal is characterized in two dimensions in terms of its linear and nonlinear responses, its noise spectra, and noise and signal power as a function of crosstrack position.

The recording medium for the simulations is set at 22 Teragrains$/\mathrm{in}^2$ (about twice today's grain densities) and the components and magnetic spacing are gauged such as to support a raw channel density of roughly $4\ \mathrm{Tb}/\mathrm{in}^2$. The results can be scaled to any density of interest, the key fundamental metric is how much customer data can be stored on each grain of the recording medium.

II. Channel Model and Database

Waveforms are derived from a simulation that uses realistic head fields and a Voronoi medium with Stoner-Wohlfarth switching [6]–[9]. The mean grain pitch is 6 nm and there are distributions in the anisotropy magnitude and angle. Magnetostatic and exchange interactions are included. The read sensitivity function is obtained by 3D-finite element modeling of a double-shielded magnetoresistive reader at several widths.

A database of 1000 oversampled waveforms was created, based on a setting in which five consecutive tracks are written in a shingled fashion, as shown in Fig. 1, each track with independent pseudorandom bit sequences of length 40950. The center track (track 3) is the track of interest. A total of 900 readback waveforms were generated with a bit length of 7.3 nm, one for each of six track pitches (from 16.1 nm to 26.1 nm in 2 nm increments), six reader widths (from 70% to 145% of a nominal reader width of 20.8 nm), and 25

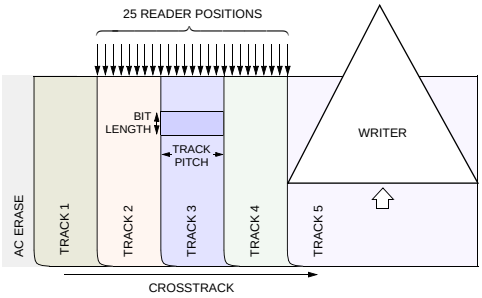

Fig. 1. We consider five shingled tracks and 25 possible reader locations.

reader positions (spanning the center three tracks at one-eighth of a track increments). The physical width of the nominal reader is 30 nm, which leads to a reader sensitivity function whose full-width half-maximum is 20.8 nm. An additional 100 readback waveforms were generated at a track pitch of 16.1 nm and 70% reader width, one for each of four additional bit lengths (5.3, 6.3, 8.3, and 9.3 nm) and the same 25 reader positions. All readback waveforms were oversampled (perfect synchronization) at two samples per bit. The same amount of white and Gaussian electronic noise was added to all readback waveforms, independent of the reader width, by adding an independent zero-mean Gaussian random variable to each oversampled readback sample, with standard deviation $\sigma_e = 0.04$. The signal to electronic noise ratio thus loses approximately 6 dB per halving of the reader width. The corresponding power of the added noise within the Nyquist band is 24.6 dB below the saturation (constant response) signal level for the centered 100%-width reader at 22.1 nm track pitch, which for that scenario is 10.1% of the total noise power (including magnetic noise).

III. Channel Characterization

Let $\mathbf{r}$ denote the row vector of the more than 80,000 oversampled samples of a given readback waveform; a linear model that accounts for contributions from all five tracks is:

$$\mathbf{r} = \sum_{n=1}^{5} \mathbf{h}_n \mathbf{A}_n + \mathbf{e},$$

where $\mathbf{h}_n$ is the oversampled linear impulse response from the n-th track to the given reader, where $\mathbf{A}_n$ is a convolution matrix for the upsampled bits written on the n-th track, and where $\mathbf{e}$ represents any modeling errors and noise. More compactly, we can write $\mathbf{r} = \mathbf{hA} + \mathbf{e}$, where $\mathbf{h} = [\mathbf{h}_1, \mathbf{h}_2, \mathbf{h}_3, \mathbf{h}_4, \mathbf{h}_5]$ is a long vector of concatenated impulse response vectors, and $\mathbf{A} = [\mathbf{A}_1^T, \mathbf{A}_2^T, \mathbf{A}_3^T, \mathbf{A}_4^T, \mathbf{A}_5^T]^T$ is a matrix of vertically stacked convolution matrices. The least-squares estimate for all five impulse responses is thus:

$$\hat{\mathbf{h}} = \mathbf{r}\mathbf{A}^T(\mathbf{A}\mathbf{A}^T)^{-1}. \quad (1)$$

For example, in Fig. 2 we show typical results of such a measurement for the case of a 70%-width reader centered over track 3, when the track pitch is 16.1 nm and the bit length is 7.3 nm. The magnitude response for track 3 is roughly 15 dB stronger than those for the neighboring tracks (tracks 2 and 4). The corresponding impulse responses are shown in the inset, with time spanning 20 bit periods. One may note how the low frequency content of track 2 is damaged by the subsequent writing of track three. Low frequencies have high demagnetizing fields and are susceptible to the stray fields from the head as the next track is written.

From the impulse response we can estimate the signal level (or saturation level) in response to a long series of one bits, or equivalently the d.c. gain, by summing all of the impulse response coefficients. In Fig. 3 we illustrate how the signal level changes as a function of the reader width, assuming that the reader is centered over the desired track, for track pitches

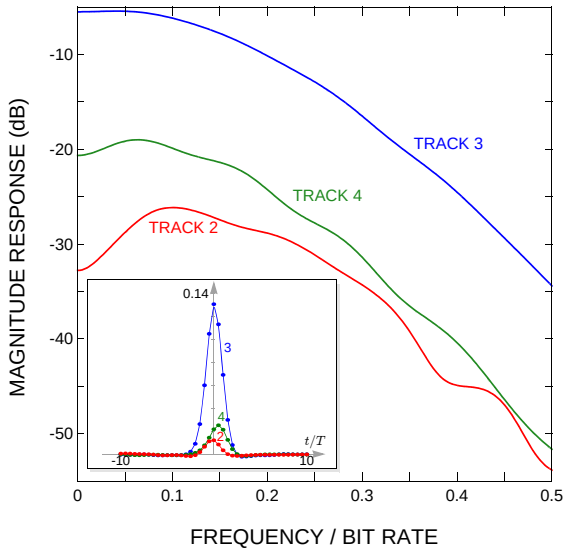

Fig. 2. The magnitude responses for a 70%-width reader centered over track 3, for three different input tracks (2, 3, and 4). The track pitch is 16.1 nm and the bit length is 7.3 nm. The inset shows the corresponding impulse responses in the time domain, spanning 20 bit periods.

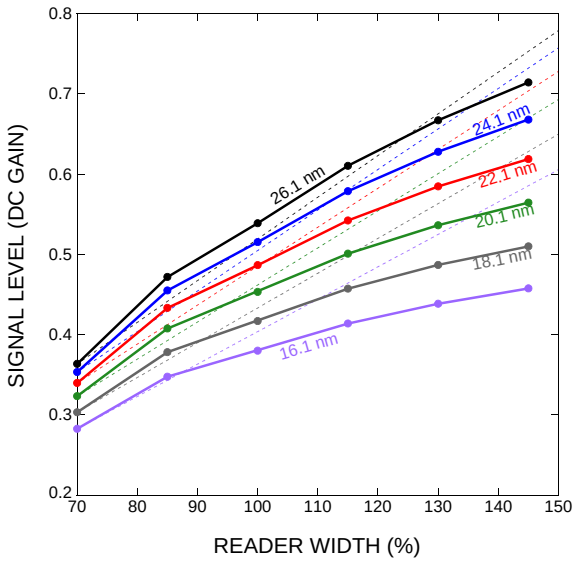

Fig. 3. Signal level for a centered reader versus reader width, for bit length 7.3 nm.

ranging from 16.1 nm to 26.1 nm. The bit length is 7.3 nm. Signal level increases nearly linearly over a wide range of reader widths. (A truly linear dependence is indicated by the dashed lines, for the sake of comparison.) Although the reader geometry is scaled linearly, the resulting sensitivity function drops more rapidly for narrow readers.

The signal (saturation) level from a neighboring track to a reader centered on a different track can be used to quantify intertrack interference (ITI). In Fig. 4 we show the ITI as a function of reader position and reader width, assuming a 16.1 nm track pitch and a 7.3 nm bit length. As expected, wider readers are seen to increase both the desired signal level and the ITI signal level. Track 5 is wider than the others because it is the last to be written, see Fig. 1, which explains its higher

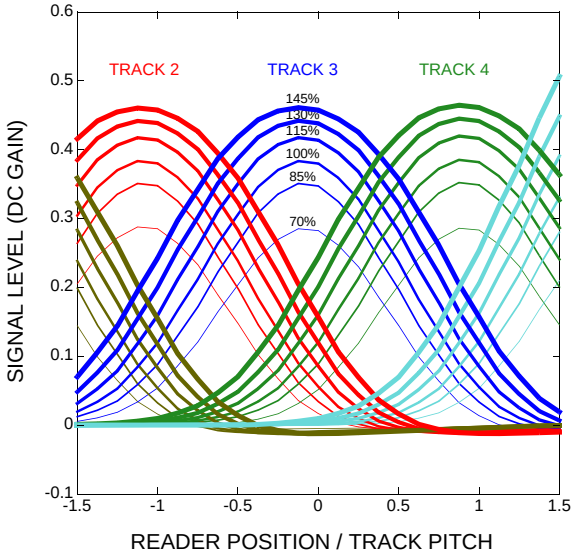

Fig. 4. Intertrack interference as quantified by signal level (DC gain), for 16.1 nm track pitch, 7.3 nm bit length, and different reader widths.

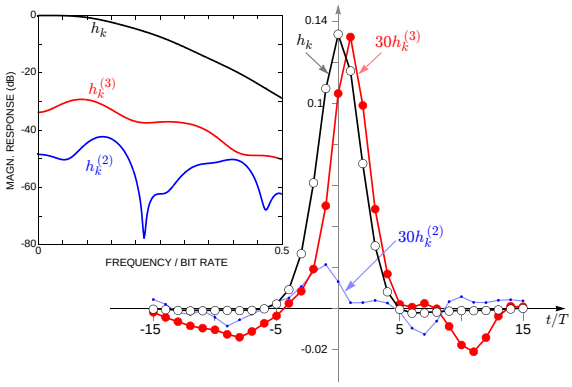

Fig. 5. A comparison of the linear impulse response h_k (open markers) and higher-order nonlinear impulse responses (closed markers) for a 70%-wide reader centered over track 3 and a track pitch of 16.1 nm. The third-order response $h_k^{(3)}$ is seen to have a similar shape as the linear impulse response, only weaker by a factor of 30. The second-order response is considerably weaker. The inset shows the corresponding magnitude responses.

signal level in Fig. 4.

Nonlinear distortion in the form of nonlinear transition shift is to be expected, since the writing process did not include any precompensation of the transition positions. A truncated Volterra model for the noiseless readback waveform from an isolated track is [10], [11]:

$$\begin{aligned} r(t) &= \sum_k a_k h(t-kT) \\ &+ \sum_k a_k a_{k-1} h^{(2)}(t-kT) \\ &+ \sum_k a_{k-1} a_k a_{k+1} h^{(3)}(t-kT), \end{aligned}$$

where $a_k \in \{\pm 1\}$ is the k-th written bit on the track, T is the bit period, $h(t)$ is the (first-order) linear impulse response, $h^{(2)}(t)$ is the second-order nonlinear response for neighboring bits, and $h^{(3)}(t)$ is the third-order nonlinear response for three consecutive bits. This third-order nonlinearity captures the impact of nonlinear distortion in which the magnetic field from bit a_k influences the formation of the transition between a_k and a_{k+1}. The nonlinear responses can be estimated via an equation like (1), but where the convolution matrices are derived not from the written bits a_k but instead from the relevant product of bits (e.g. $a_k a_{k-1}$ for $h^{(2)}(t)$, and $a_{k-1}a_k a_{k+1}$ for $h^{(3)}(t)$.) A comparison of these three Volterra kernels is shown in Fig. 5, for the case of a 70%-width reader centered over track 3, with track pitch 16.1 nm and bit length 7.3 nm. The oversampled linear impulse response h_k is seen to dominate by more than 30 dB. The oversampled third-order response $h_k^{(3)}$ is the next-largest; when scaled by a factor of 30 it shares nearly the same height and shape as the linear impulse response. The second-order response is significantly weaker.

Once the impulse responses to a given reader have been estimated, we can predict the corresponding sampled readback waveform by convolving the known bit sequences written on all five tracks with the corresponding linear impulse response estimates, or equivalently in terms of the notation of (1), according to $\hat{\mathbf{r}} = \hat{\mathbf{h}}\mathbf{A}$. Any error $\mathbf{e} = \mathbf{r} - \hat{\mathbf{r}}$ between this prediction and the actual samples (before adding electronic noise) can be attributed to media noise and nonlinear distortion, the latter being a much smaller contributor. If $\sigma^2_{\text{media}} = \|\mathbf{e}\|^2 / L$ denotes an estimate of the variance of this media noise, where L is the length of $\mathbf{e}$, and if H_0 denote the DC gain, then the SNR (with respect to the DC gain) can be computed as $SNR = H_0^2/(\sigma_m^2 + \sigma_e^2/2)$, where we use $\sigma_e = 0.04$ for the added electronic noise. Observe that this measure of SNR is independent of ITI, as might result from either an isolated track or for the case when ITI is perfectly cancelled.

The dependence of SNR on reader width is illustrated in Fig. 6. The solid curves include the electronic noise, while the dashed curves have no electronic noise ($\sigma_e = 0$). In all cases we see an optimum reader width that trades off the opposing goals of capturing as much desired signal energy (using a wide reader) and avoiding the media noise at the track edges (using a narrow reader).

The power-spectral density for the media noise $\mathbf{e} = \mathbf{r} - \hat{\mathbf{h}}\mathbf{A}$ is shown in Fig. 7 for a centered reader over a track with pitch 26.1 nm. The upper curve is for a 145% reader width, and the lower curve is for the 70% reader width. The spectrum of the media noise is clearly seen to be shaped by the reader response, in contrast to the spectrum of the electronic noise.

The media noise $\mathbf{e} = \mathbf{r} - \hat{\mathbf{h}}\mathbf{A}$ (see (1)) is computed by subtracting the linear ISI and ITI contributions from the readback waveform. The variance of each media noise sample is time-varying and data dependent. This time variance and data dependence is captured by an *instantaneous* measure $\sigma^2_{\text{media},k}$ of media noise variance at each time k, conditioned on knowledge of the written bits. Galbraith *et al.* proposed the following linear model for this time-varying data-dependent variance [12]:

$$\hat{\sigma}^2_{\text{media},k} = \sigma_0^2 + \sum_i t_i w_{k-i},$$

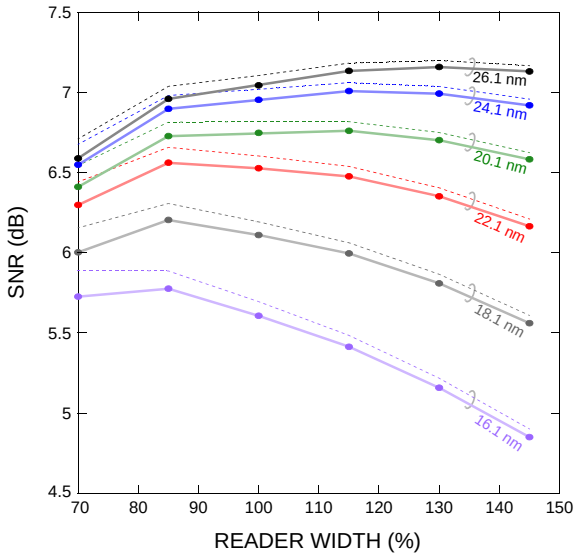

Fig. 6. SNR versus reader width, for a centered reader and bit length 7.3 nm. The dashed curves are for the case of no noise ($\sigma_e = 0$), while the solid curves are with the electronic noise ($\sigma_e = 0.04$).

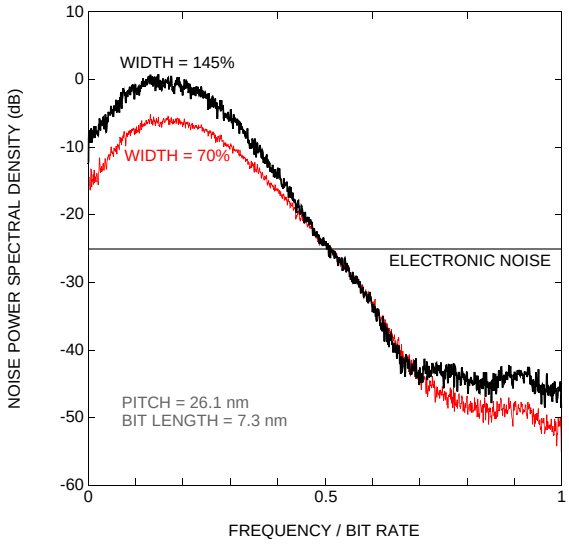

Fig. 7. Media noise power spectral densities for two different reader widths, assuming a centered reader, a track pitch of 26.1 nm, and bit length 7.3 nm. The electronic noise level is shown for comparison.

where the first term σ_0^2 is independent of the presence of a transition, representing the non-transition media noise, and where the second term represents the transition-dependent media noise, expressed in terms of the transition sequence $t_k = |a_k - a_{k+1}|/2 \in \{0, 1\}$ and the so-called transition-noise variance response sequence w_k.

With $\{\sigma^2_{\text{media},k}\}$ measured experimentally, [12] proposed to estimate the parameters σ_0^2 and $\{w_k\}$ so as to minimize $\sum_k |\hat{\sigma}^2_{\text{media},k} - \sigma^2_{\text{media},k}|^2$, and to use the resulting estimates to quantify the transition noise power and the nontransition noise power. Fig. 8 shows sample results this measurement technique for the case of a 70%-width reader, a track pitch of 22.1 nm, and a bit length of 7.3 nm. The figure shows the relative power of four disturbances as a function of the

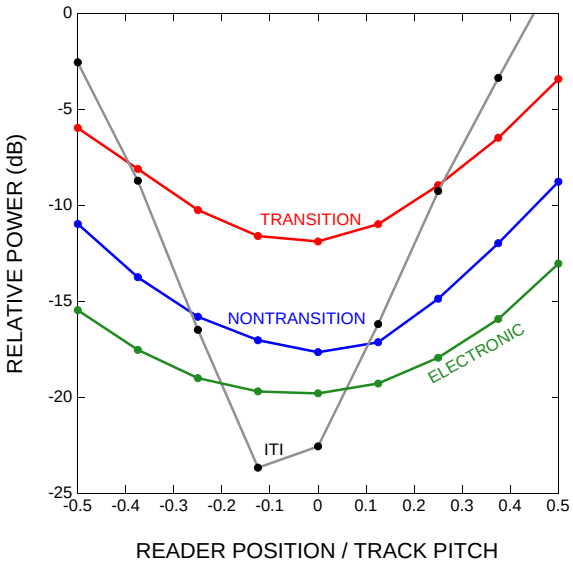

Fig. 8. Dependence of noise on crosstrack reader position.

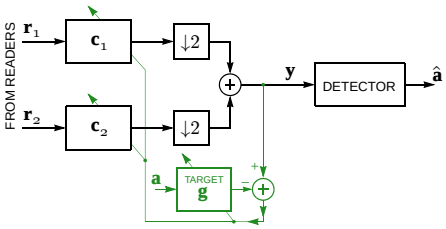

Fig. 9. A single-track detector preceded by a pair of fractionally spaced equalizers, whose outputs are downsampled and added. The equalizers and monic-constrained target are jointly designed to minimize mean-squared error.

crosstrack reader position: the ITI power, the transition noise power, the nontransition noise power, and the electronic noise power. All powers are normalized by the power of the desired signal for the main track, so that a value of 0 dB means that the noise power is equal to the signal power.

IV. Multi-Reader Detection

We limit consideration to single-track detectors of the form illustrated in Fig. 9. The two oversampled readback waveforms from the two readers are separately equalized by a pair of fractionally spaced equalizers, each with N_c coefficients, and then added together. The pair of equalizers and the one-dimensional monic-constrained target $\mathbf{g} = [1, g_1, \ldots g_\mu]$ with memory μ are jointly optimized using standard techniques so as to minimize mean-squared error [13], so that subsequent processing can use conventional one-dimensional Viterbi [14] and Bahl, Cocke, Jelinek, and Raviv (BCJR) detectors [15].

In Fig. 10 we show bathtub curves for the case of two 70%-width readers whose crosstrack spacing (normalized by the track pitch) is $1/8$, based on the bit-error rate after a hard-output Viterbi detector (with no noise prediction).

The optimum spacing between two readers depends on many factors, but roughly boils down to a compromise between a desire to use a small spacing, so as to avoid the

noise and ITI at the track edges, and a desire to use a large spacing, to reduce transition media noise via averaging, and to provide robustness to misregistration. In Fig. 11 we illustrate this tradeoff via a family of bathtub curves, for the case of two 70% readers and a track pitch of 18.1 nm. Six curves are shown, for normalized reader spacings (normalized by the track pitch) ranging from zero to 5/8 in increments of 1/8. The narrowest bathtub curve corresponds to a zero crosstrack spacing; the two corresponding readback waveforms will thus have precisely the same media noise, differing only because the added electronic noise is independent. Slightly better BER performance at the bottom of the curve is achieved by a normalized spacing of 1/8. More significant, however, is the greater width of the resulting bathtub curve, making this configuration more robust to misregistration. Further increasing the spacing beyond 1/8 results in an even wider curve, albeit with a somewhat larger minimum value. If we were to choose the spacing to minimize the BER value at the bottom of the curve, ignoring the width of the curve, we would choose 1/8.

V. Symmetric Information Rate

The bit-error rate after Viterbi detection is a useful performance metric when optimizing the multireader geometry for a given track pitch and bit length, but it cannot be used to optimize the track pitch and bit length parameters themselves. Here we propose a more comprehensive metric that can be used to simultaneously optimize all parameters. An ideal optimization metric would be the Shannon capacity, since it would upper bound the areal density for any practical system. Instead, because the Shannon capacity is not known for this channel, we propose to use the symmetric information rate (SIR) between the input sequence $\mathbf{a}$ of written bits on the home track and the output sequence $\mathbf{y}$ after the equalizer(s). The SIR is the mutual information rate $I(\mathbf{a};\mathbf{y})$ between $\mathbf{a}$ and $\mathbf{y}$ under the constraint that the written bits are independent and uniformly distributed (i.i.d.) random variables, namely:

$$SIR = h(\mathbf{y}) - h(\mathbf{y}|\mathbf{a}), \tag{2}$$

where $h(\mathbf{y})$ is the entropy rate of the equalizer output, and $h(\mathbf{y}|\mathbf{a})$ is the conditional entropy rate of the output, given $\mathbf{a}$.

The units of SIR are information bits, and can be interpreted as a bound on the average number of user bits per written bit. Therefore, the areal density (in units of bits per grain) can be computed as SIR/G, where G is the average number of grains per written bit, and can be computed from the track pitch, bit length, and grain density. (For example, a track pitch of 16.1 nm, bit length of 7.3 nm, and 22 Teragrains/in^2 leads to $G = 4.01$ grains/written bit.) Like Shannon capacity, the SIR is a property of the channel itself, and is not tied to any particular coding scheme or decoding strategy. The SIR thus provides a useful benchmark for achievable storage densities for systems that use single-track detection with multiple readers.

Let us write the equalizer output as:

$$\mathbf{y} = \mathbf{s}(\mathbf{a}) + \mathbf{n}(\mathbf{a}),$$

where without loss of generality we define the k-th component of $\mathbf{s}(\mathbf{a})$ as the linear convolution $s_k = \sum_{i=0}^{\mu} g_i a_{k-i}$, where $\{g_0, \ldots g_\mu\}$ are the target coefficients; any nonlinearities or other effects can then be lumped into the additive signal-dependent noise, defined by $\mathbf{n}(\mathbf{a}) \triangleq \mathbf{y} - \mathbf{s}(\mathbf{a})$. Suppose the noise is data-dependent order-L autoregressive (AR) and Gaussian of the form [16]:

$$n_k(\mathbf{a}) = \sigma_k(\mathbf{a}_k)u_k + \sum_{i=1}^{L} p_{i,k}(\mathbf{a}_k)n_{k-i}, \tag{3}$$

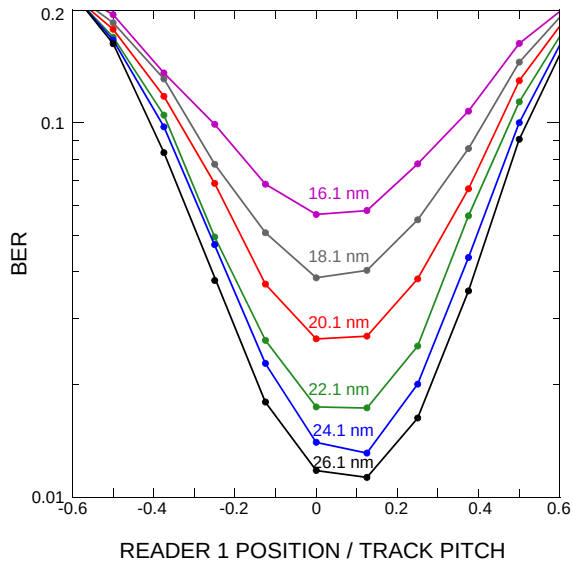

Fig. 10. Bathtub curves for two 70%-width readers with crosstrack spacing (normalized by track pitch) of 1/8, based on a 4-state Viterbi detector. The equalizers and target are optimized anew for each point on each curve.

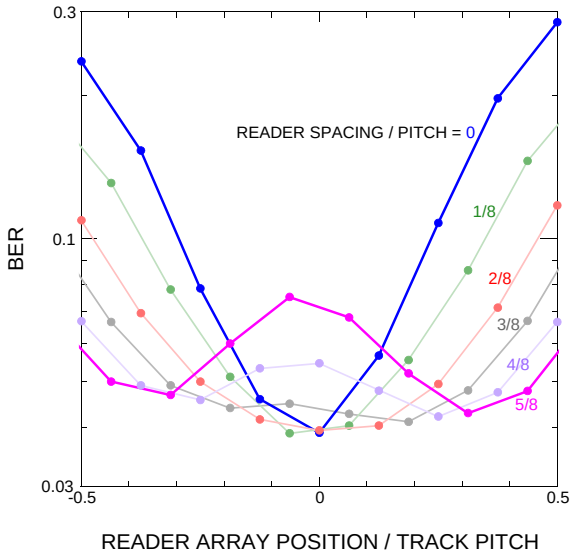

Fig. 11. Impact of spacing between two readers on the bathtub curve. The horizontal axis is the position of the array center (i.e., the midpoint between the two readers). The track pitch is 18.1 nm and the bit length is 7.3 nm. Closely spaced readers yield the lowest BER, but wider spacing is more robust to misregistration.

where $\{u_k\}$ is an i.i.d. sequence of zero-mean unit-variance Gaussian random variables, and where $\sigma_k(\mathbf{a}_k)$ and $\mathbf{p}_k(\mathbf{a}_k) = [p_{1,k}(\mathbf{a}_k), \ldots p_{L,k}(\mathbf{a}_k)]$ are the data-dependent time-varying AR parameters that depend at time k only on the $\mu+1$ written bits $\mathbf{a}_k \triangleq [a_k \ldots a_{k-\mu}]$. Applying the noise of (3) to a time-varying linear predictor of the form $\hat{n}_k = \sum_{i=1}^{L} p_{i,k}(\mathbf{a}_k) n_{k-i}$ with knowledge of $\mathbf{a}$ would then lead to an uncorrelated prediction error sequence $e_k = n_k - \hat{n}_k = \sigma_k(\mathbf{a}_k)u_k$.

We now examine how to compute the second of the two terms in (2), namely $h(\mathbf{y}|\mathbf{a})$. When the AR model of (3) is exact, the conditional entropy $h(\mathbf{y}|\mathbf{a})$ can be computed exactly. Considering that $h(\mathbf{y}|\mathbf{a})$ is a measure of uncertainty in $\mathbf{y}$ given knowledge of $\mathbf{a}$, and further that knowledge of $\mathbf{a}$ and the AR parameters enables us to extract $\mathbf{e}$ through linear prediction, it follows that the conditional entropy reduces to:

$$h(\mathbf{y}|\mathbf{a}) = h(\mathbf{e}) = \frac{1}{2}\log_2(2\pi e\bar{\sigma^2}),$$

where $\bar{\sigma^2} = 2^{E(\log_2 \sigma_k^2(\mathbf{a}_k))}$. This further reduces to $h(\mathbf{n}) = \frac{1}{2}\log_2(2\pi e\sigma^2)$, as expected, in the special case when the noise $\mathbf{n}$ is AWGN and independent of $\mathbf{a}$.

When the noise is autoregressive according to (3), the first term $h(\mathbf{y})$ in (2), the entropy of the equalizer output, can also be computed exactly; it can be computed using the forward recursion of the BCJR algorithm, as explained in [17], which operates on a $2^{\mu+1+L}$-state trellis.

In the spirit of [18], data-dependent noise prediction can still be used to estimate the conditional entropy $h(\mathbf{y}|\mathbf{a})$, and the forward recursion of BCJR can still be used to estimate $h(\mathbf{y})$, even when the noise does not strictly follow the autoregressive model of (3). Strategies for empirically estimating $\sigma_k(\mathbf{a}_k)$ and $\mathbf{p}_k(\mathbf{a}_k)$ are discussed in [18].

VI. Optimization Results

We first assume a bit length of 7.3 nm and optimize all other parameters. We then fix these remaining parameters and optimize bit length. In particular, for the 7.3 nm bit length and every track pitch and reader geometry, the corresponding pair of readback waveforms was processed according to Sect. 4, and both the SIR and BER computed. An exhaustive search over all possible candidate geometries was then performed. A similar exhaustive search was also performed for a single-reader system.

Results are shown in Fig. 12, where we plot BER after a standard 4-state Viterbi detection (without noise prediction) versus track pitch. Every parameter of the system (bit geometry, reader geometry, equalizer, and target) is optimized separately for each point in the curves so as to minimize the resulting BER. The two-reader system is seen to offer up to an 11% increase in areal density over the single-reader system.

A similar search was performed so as to maximize the SIR in units of bits per grain, rather than to minimize BER. The results are shown in Fig. 13, where we plot versus track pitch the optimized areal density versus track pitch. The units on the left are $\mathrm{Tb/in^2}$, while the units on the right are bits/grain. As before, every parameter of the system (bit geometry, reader geometry, equalizer, and target) is optimized separately for each point in the curves so as to maximize the areal density. A maximum areal density of at 4.8 $\mathrm{Tb/in^2}$ (or 0.22 bits/grain) is achieved at a track pitch of 16.1 nm, with reader widths 23.9 nm and 14.6 nm and center spacing 2 nm. The corresponding code rate is 0.79. Compared to an optimized single-reader system, the second reader provides an 5% increase in areal density.

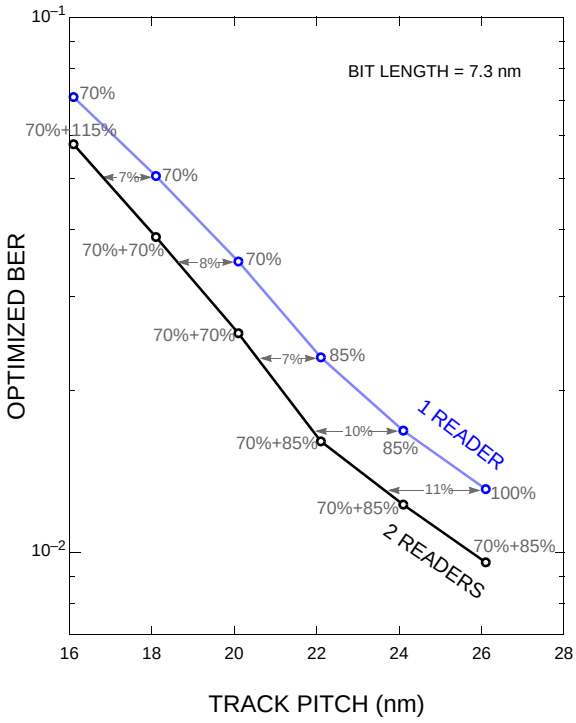

Fig. 12. Optimized BER versus track pitch, for bit length 7.3 nm. At each point the equalizers, target, reader widths, reader spacing, and position are optimized to minimize BER. The optimum reader widths are indicated at each point.

We next examine performance as a function of bit length. Up to now we have added the same amount of electronic noise to each readback waveform, regardless of the reader width. But when varying the bit length while keeping the rotational speed of the medium fixed, we must scale the noise standard deviation to account for the change in bit rate. In particular, to be consistent with the choice of $\sigma_e = 0.04$ when the bit length was $L_0 = 7.3$ nm, the electronic noise standard deviation value as a function of bit length L_b is $\sigma_e = 0.04\sqrt{L_0/L_b}$. With the track pitch fixed at its optimal value (16.1 nm), and while keeping the reader geometry fixed at two 70%-wide readers with a 1/8-pitch spacing, we computed the SIR as a function of bit length. The results are shown in 14 for the case of one and two readers. The one-reader system achieves a maximum areal density at 8.3 nm, while the two-reader system achieves a maximum at 7.3 nm.

VII. Conclusions

The simulated waveforms were analyzed in terms of their linear and nonlinear characteristics, as well as their noise properties, and were shown to be realistic and representative. The simulated waveforms enabled a comprehensive exhaustive

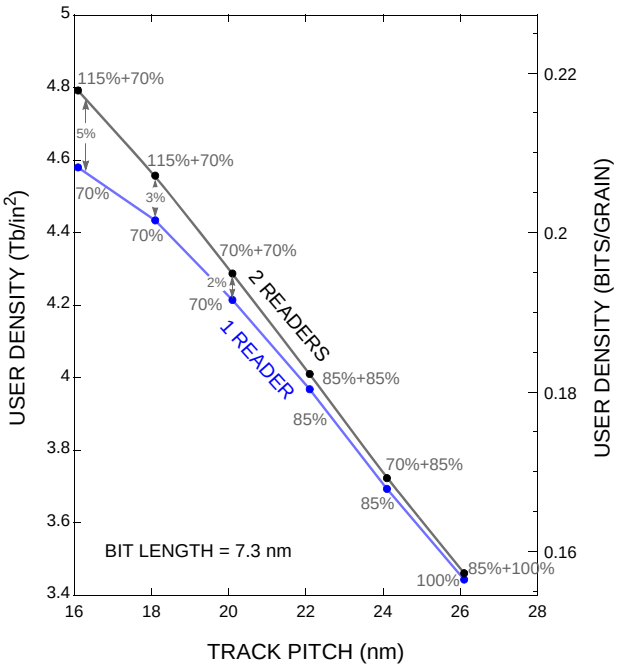

Fig. 13. Optimized areal density versus track pitch, as predicted by SIR, for bit length 7.3 nm. The units on the left axis are $\mathrm{Tb/in^2}$, while the units on the right are user bits per grain.

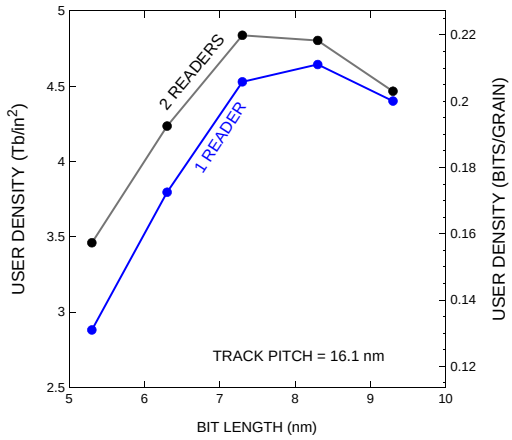

Fig. 14. Areal density as a function of bit length, as predicted by SIR. The reader geometry was fixed at two 70%-wide readers with a 1/8-pitch spacing, and the track pitch is 16.1 nm.

search for optimizing the geometry of multiple readers so as to maximize density. Moving from one to two readers was shown to increase the maximal areal density by 5%. Further gains in areal density can be expected by relaxing the constraints of the single-track reader architecture considered here, e.g., by considering multiple-track detectors based on a joint Viterbi or other trellis-based detector; by employing modulation codes controlling both downtrack and crosstrack transitions; by employing crosstrack media-noise processing such as data-dependent noise prediction. Our optimization results are limited by the range of parameters considered, notably the fact that they were based on zero skew, and also the limited range of track pitches and bit lengths considered. A broader optimization criterion that accounts for both skew and track misregistration will likely lead to different optimization results.

Acknowledgments

The authors gratefully acknowledge the guidance and support of Roger Wood and Hiroshi Mutoh. This work was supported in part by the IDEMA ASTC, USA, and the Storage Research Consortium, Japan, and by NSF grant CCF-1314147.

References

[1] R. Wood, M. Williams, A. Kavcic, and J. Miles, "The feasibility of magnetic recording at 10 Terabits per square inch on conventional media," *Magnetics, IEEE Transactions on*, vol. 45, no. 2, pp. 917–923, Feb 2009.

[2] ASTC, *ASTC Technology Roadmap: 2014 v8*, 2014. [Online]. Available: http://www.idema.org/

[3] S. Dahandeh, M. F. Erden, and R. Wood, "Areal-density gains and technology roadmap for two-dimensional magnetic recording," in *TMRC, 2015*, Aug 2015, p. Paper F1.

[4] R. Wood, R. Galbraith, and J. Coker, "2-D magnetic recording: Progress and evolution," *Magnetics, IEEE Transactions on*, vol. 51, no. 4, pp. 1–7, April 2015.

[5] M. Igarashi, M. Hara, A. Nakamura, and Y. Sugita, "Micromagnetic simulation of magnetic cluster, thermal activation volume, and medium noise in perpendicular recording media," *Magnetics, IEEE Transactions on*, vol. 39, no. 4, pp. 1897–1901, July 2003.

[6] B. Vasic, M. Khatami, Y. Nakamura, Y. Okamoto, Y. Kanai, J. Barry, S. McLaughlin, and E. Sadeghian, "A study of TDMR signal processing opportunities based on quasi-micromagnetic simulations," *Magnetics, IEEE Transactions on*, vol. 51, no. 4, pp. 1–7, April 2015.

[7] M. Yamashita, Y. Okamoto, Y. Nakamura, H. Osawa, K. Miura, S. Greaves, H. Aoi, Y. Kanai, and H. Muraoka, "Modeling of writing process for two-dimensional magnetic recording and performance evaluation of two-dimensional neural network equalizer," *Magnetics, IEEE Transactions on*, vol. 48, no. 11, pp. 4586–4589, Nov 2012.

[8] Y. Yamashita, Y. Okamoto, Y. Nakamura, H. Osawa, S. J. Greaves, and H. Muraoka, "Performance evaluation of neuro-ITI canceller using a modified writing process for TDMR," *Electron., IEICE Trans.*, vol. E96C, no. 12, pp. 1504–1507, December 2013.

[9] Y. Kanai, Y. Jinbo, T. Tsukamoto, S. Greaves, K. Yoshida, and H. Muraoka, "Finite-element and micromagnetic modeling of write heads for shingled recording," *Magnetics, IEEE Transactions on*, vol. 46, no. 3, pp. 715–721, March 2010.

[10] D. Palmer, P. Ziperovich, R. Wood, and T. Howell, "Identification of nonlinear write effects using pseudorandom sequences," *Magnetics, IEEE Transactions on*, vol. 23, no. 5, pp. 2377–2379, Sep 1987.

[11] R. Hermann, "Volterra modeling of digital magnetic saturation recording channels," *Magnetics, IEEE Transactions on*, vol. 26, no. 5, pp. 2125–2127, Sep 1990.

[12] R. Galbraith, W. Hanson, B. Lengsfield, T. Oenning, J. Park, and M. Salo, "Noise characterization in high-areal density perpendicular and shingled magnetic recording," *Magnetics, IEEE Transactions on*, vol. 50, no. 3, pp. 67–73, March 2014.

[13] J. Moon and W. Zeng, "Equalization for maximum likelihood detectors," *Magnetics, IEEE Transactions on*, vol. 31, no. 2, pp. 1083–1088, March 1995.

[14] J. Forney, G.D., "The Viterbi algorithm," *Proceedings of the IEEE*, vol. 61, no. 3, pp. 268–278, March 1973.

[15] L. Bahl, J. Cocke, F. Jelinek, and J. Raviv, "Optimal decoding of linear codes for minimizing symbol error rate (corresp.)," *Information Theory, IEEE Transactions on*, vol. 20, no. 2, pp. 284–287, Mar 1974.

[16] A. Kavcic and J. M. F. Moura, "The Viterbi algorithm and Markov noise memory," *IEEE Transactions on Information Theory*, vol. 46, no. 1, pp. 291–301, 2000. [Online]. Available: http://dx.doi.org/10.1109/18.817531

[17] D. Arnold, H.-A. Loeliger, P. Vontobel, A. Kavcic, and W. Zeng, "Simulation-based computation of information rates for channels with memory," *Information Theory, IEEE Transactions on*, vol. 52, no. 8, pp. 3498–3508, Aug 2006.

[18] J. Moon and J. Park, "Pattern-dependent noise prediction in signal-dependent noise," *IEEE Journal on Selected Areas in Communications*, vol. 19, no. 4, pp. 730–743, 2001. [Online]. Available: http://dx.doi.org/10.1109/49.920181